

Cold and ultracold NH–NH collisions: The field-free case

Liesbeth M. C. Janssen,¹ Piotr S. Żuchowski,² Ad van der Avoird,¹ Jeremy M. Hutson,^{2,*} and Gerrit C. Groenenboom^{1,†}

¹*Radboud University Nijmegen, Institute for Molecules and Materials,
Heyendaalseweg 135, 6525 AJ Nijmegen, The Netherlands*

²*Department of Chemistry, Durham University,
South Road, Durham, DH1 3LE, United Kingdom*

(Dated: March 8, 2011)

Abstract

We present elastic and inelastic spin-changing cross sections for cold and ultracold $\text{NH}(X^3\Sigma^-) + \text{NH}(X^3\Sigma^-)$ collisions, obtained from full quantum scattering calculations on an accurate *ab initio* quintet potential-energy surface. Although we consider only collisions in zero field, we focus on the cross sections relevant for magnetic trapping experiments. It is shown that evaporative cooling of both fermionic ^{14}NH and bosonic ^{15}NH is likely to be successful for hyperfine states that allow for *s*-wave collisions. The calculated cross sections are very sensitive to the details of the interaction potential, due to the presence of (quasi-)bound state resonances. The remaining inaccuracy of the *ab initio* potential-energy surface therefore gives rise to an uncertainty in the numerical cross-section values. However, based on a sampling of the uncertainty range of the *ab initio* calculations, we conclude that the exact potential is likely to be such that the elastic-to-inelastic cross-section ratio is sufficiently large to achieve efficient evaporative cooling. This likelihood is only weakly dependent on the size of the channel basis set used in the scattering calculations.

*Electronic mail: J.M.Hutson@durham.ac.uk

†Electronic mail: Gerritg@theochem.ru.nl

I. INTRODUCTION

Cold ($T < 1$ K) and ultracold ($T < 1$ mK) molecules offer a wide variety of applications in condensed-matter physics [1], high-precision spectroscopy [2–4], physical chemistry [5–9], and quantum computing [10, 11]. In the last few years, techniques have been developed that either form (ultra)cold molecules by pairing up pre-cooled atoms, e.g. by photoassociation [12] or Feshbach association [13], or by cooling the molecules directly. Examples of the latter approach include buffer-gas cooling [14] and Stark deceleration [15].

A promising candidate for direct-cooling experiments is the NH biradical. NH in its electronic $X^3\Sigma^-$ ground state has been cooled from room temperature using a helium buffer gas and trapped in a magnetic field [8, 16–18]. Stark deceleration and electrostatic trapping experiments have been performed on metastable $\text{NH}(a^1\Delta)$, which, in contrast to the $X^3\Sigma^-$ ground state, exhibits a linear Stark effect. The decelerated $\text{NH}(a^1\Delta)$ molecules can be converted to the ground state by excitation of the $A^3\Pi \leftarrow a^1\Delta$ transition followed by spontaneous emission [19, 20]. The resulting $\text{NH}(X^3\Sigma^-)$ molecules may subsequently be accumulated in a magnetic trap.

Direct-cooling techniques for NH are currently limited to temperatures of a few hundred mK. Producing NH molecules in the ultracold regime requires a second-stage cooling mechanism, e.g. sympathetic cooling with an ultracold atomic gas [21–25] or evaporative cooling. The latter process relies on elastic, thermalizing $\text{NH} + \text{NH}$ collisions as the magnetic trap depth is gradually reduced. Inelastic spin-changing collisions lead to immediate trap loss and are therefore unfavorable. It is generally accepted that, in order to achieve evaporative cooling, elastic collisions should be much more efficient than inelastic ones. More specifically, a Monte Carlo study on evaporative cooling of cesium atoms indicated that the ratio between elastic and inelastic collision rates should be greater than 150 [26]. Although evaporative cooling of NH might work with a lower ratio, it will be assumed that 150 is also the minimum required value for $\text{NH} + \text{NH}$ collisions.

For two magnetically trapped $\text{NH}(X^3\Sigma^-)$ molecules, the collision complex is in the low-field seeking $|S = 2, M_S = 2\rangle$ quintet spin state, with S denoting the total electronic spin and M_S its projection on the magnetic-field axis. Inelastic transitions may change either the M_S quantum number of the quintet state, or the total spin S to produce singlet or triplet complexes. The $S = 0$ and 1 dimer spin states are chemically reactive [27–29] and could be

of interest in cold controlled chemistry experiments [9].

A rigorous calculation of elastic and inelastic cross sections requires a full quantum coupled-channels method. In the case of NH–NH, however, the strong anisotropy of the interaction potentials and the open-shell nature of the monomers gives rise to a very large number of channels, making the calculation extremely challenging. In a recent study by Tscherbul *et al.* [30] on the iso-electronic $\text{O}_2(X^3\Sigma_g^-) - \text{O}_2(X^3\Sigma_g^-)$ system, close-coupling calculations were performed that included up to 2526 channels, yielding cross sections converged to within 10%. These calculations were carried out in a fully decoupled channel basis to study collisions in the presence of an external magnetic field. It was noted, however, that the true O_2 – O_2 interaction potential is likely to be more anisotropic than the potential used in their work, thus implying that even more channels would be needed. Other quantum scattering studies on O_2 – O_2 include those by Avdeenkov and Bohn [31] and Pérez-Ríos *et al.* [32]. In the work of Avdeenkov and Bohn, field-free collisions were studied using a total angular momentum representation, thereby reducing the total number of channels to 836. The rotational basis-set size used in these calculations was, however, smaller than that used in Ref. [30]. Pérez-Ríos *et al.* also employed a total angular momentum basis, but the O_2 monomers were treated as closed-shell molecules. This allowed them to reduce the number of channels to 300.

To our knowledge, only one theoretical study has been reported for the NH–NH system. Kajita [33] employed the Born approximation, distorted-wave Born approximation, and classical path method to calculate elastic and inelastic cross sections at energies ranging from 1 μK to 10 K, and found that evaporative cooling of NH is likely to be feasible. It must be noted, however, that only the electric dipole-dipole and magnetic dipole-dipole interactions were considered in these calculations.

The aim of the present work is to obtain cold and ultracold NH + NH collision cross sections from rigorous quantum scattering calculations on an accurate *ab initio* quintet potential-energy surface. We include intramolecular spin-spin, spin-rotation, and intermolecular magnetic dipole-dipole coupling in the dynamics. In addition, we seek to address the issue of dealing with very large basis sets in order to converge the scattering results, a problem that is general for open-shell systems with relatively deep potential energy wells. For this purpose, we have employed a total angular momentum representation to perform the scattering calculations, assuming zero field. Collisions in a magnetic field are discussed

in a separate publication [34]. It will be shown that, within the uncertainty limits of the interaction potential, even an unconverged basis set can provide meaningful results.

This paper is organized as follows. In Sec. II, we discuss the scattering Hamiltonian and channel basis-set functions, followed by the details of the cross-section calculations. Results are presented in Sec. III A. In Secs. III B and III C, we provide a comprehensive discussion on the accuracy of our calculated cross sections. Conclusive remarks are given in Sec. IV.

II. THEORY

A. Hamiltonian and channel basis functions

We consider the case of two colliding $\text{NH}(^3\Sigma^-)$ molecules in the absence of an external field and treat the monomers as rigid rotors. We use a space-fixed coordinate frame to describe the collision complex. The relevant Jacobi coordinates are the intermolecular vector \mathbf{R} that connects the centers of mass of molecules A and B , and the polar angles $\omega_i = (\theta_i, \phi_i)$ of the two monomers ($i = A, B$). We will neglect hyperfine coupling and assume that both monomers are in their nuclear-spin stretched states $|I, M_I = I\rangle$, with $I = I_N + I_H$ denoting the maximum total nuclear spin and M_I its laboratory-frame projection. For fermionic ^{14}NH the maximum nuclear spin is $I = 3/2$ and for bosonic ^{15}NH we have $I = 1$.

The scattering Hamiltonian for NH-NH can be written as

$$\hat{H} = -\frac{\hbar^2}{2\mu R} \frac{\partial^2}{\partial R^2} R + \frac{\hat{L}^2}{2\mu R^2} + V_S(\mathbf{R}, \omega_A, \omega_B) + V_{\text{magn.dip}}(\mathbf{R}, \hat{\mathbf{S}}_A, \hat{\mathbf{S}}_B) + \hat{H}_A + \hat{H}_B, \quad (1)$$

where μ is the reduced mass of the complex, R is the length of the vector \mathbf{R} , \hat{L}^2 is the angular momentum operator associated with rotation of \mathbf{R} , $V_S(\mathbf{R}, \omega_A, \omega_B)$ is the potential-energy surface for total spin S , $V_{\text{magn.dip}}(\mathbf{R}, \hat{\mathbf{S}}_A, \hat{\mathbf{S}}_B)$ is the intermolecular magnetic dipole interaction between the two triplet spins, and \hat{H}_A and \hat{H}_B are the Hamiltonians of the individual monomers. The magnetic dipole term is given by

$$V_{\text{magn.dip}}(\mathbf{R}, \hat{\mathbf{S}}_A, \hat{\mathbf{S}}_B) = -\sqrt{6} g_S^2 \mu_B^2 \frac{\alpha^2}{R^3} \sum_q (-1)^q C_{2,-q}(\Omega) [\hat{\mathbf{S}}_A \otimes \hat{\mathbf{S}}_B]_q^{(2)}, \quad (2)$$

where $g_S \approx 2.0023$ is the electron g -factor, μ_B is the Bohr magneton, α is the fine-structure constant, $C_{2,-q}$ is a Racah-normalized spherical harmonic, $\Omega = (\Theta, \Phi)$ describes the orientation of \mathbf{R} in the space-fixed frame, and the factor in square brackets represents the tensorial

product of the monomer spin operators $\hat{\mathbf{S}}_A$ and $\hat{\mathbf{S}}_B$. The monomer operators \hat{H}_i each contain a rotation, spin-rotation, and intramolecular spin-spin term:

$$\hat{H}_i = B_0 \hat{N}_i^2 + \gamma \hat{\mathbf{N}}_i \cdot \hat{\mathbf{S}}_i + \frac{2}{3} \sqrt{6} \lambda_{\text{ss}} \sum_q (-1)^q C_{2,-q}(\omega_i) [\hat{\mathbf{S}}_i \otimes \hat{\mathbf{S}}_i]_q^{(2)}, \quad (3)$$

with \hat{N}_i denoting the rotational angular momentum operator of monomer i . For brevity, we will denote the intramolecular spin-spin operator as $\hat{V}_{\text{ss}}^{(i)}$. The numerical values for the rotational, spin-rotation, and spin-spin constants are $B_0 = 16.343275 \text{ cm}^{-1}$, $\gamma = -0.05486 \text{ cm}^{-1}$, and $\lambda_{\text{ss}} = 0.91989 \text{ cm}^{-1}$ [35] for ^{14}NH , and, by scaling with the isotope mass (see e.g. p. 239 of Ref. [36]), we obtain $B_0 = 16.270340 \text{ cm}^{-1}$, $\gamma = -0.05460 \text{ cm}^{-1}$, and $\lambda_{\text{ss}} = 0.91989 \text{ cm}^{-1}$ for ^{15}NH .

For the interaction potential $V_S(\mathbf{R}, \omega_A, \omega_B)$ we take the $S = 2$ *ab initio* surface of Ref. [28]. This spin state corresponds to the case where both molecules are in their magnetically trapped (spin-stretched) states. Although the potential is based on the Jacobi coordinates for $^{14}\text{NH} - ^{14}\text{NH}$, we use the same surface for the $^{15}\text{NH} - ^{15}\text{NH}$ isotope. This approximation is very reasonable since the center of mass of ^{15}NH is shifted by only $0.008 a_0$ with respect to that of ^{14}NH . We have verified that, at the equilibrium distance of the complex, this would give a maximum error of 2.2% in the $^{15}\text{NH} - ^{15}\text{NH}$ potential, which falls within the uncertainty range of the *ab initio* data. Following Ref. [37], we expand the quintet potential in terms of spherical harmonics $Y_{L,M}$ of degree L and order M :

$$V(\mathbf{R}, \omega_A, \omega_B) = \sum_{L_A, L_B, L_{AB}} v_{L_A, L_B, L_{AB}}(R) A_{L_A, L_B, L_{AB}}(\Omega, \omega_A, \omega_B), \quad (4)$$

$$A_{L_A, L_B, L_{AB}}(\Omega, \omega_A, \omega_B) = \sum_{M_A, M_B, M_{AB}} \langle L_A M_A L_B M_B | L_{AB} M_{AB} \rangle \times Y_{L_A, M_A}(\omega_A) Y_{L_B, M_B}(\omega_B) Y_{L_{AB}, M_{AB}}^*(\Omega), \quad (5)$$

where $\langle L_A M_A L_B M_B | L_{AB} M_{AB} \rangle$ is a Clebsch-Gordan coefficient and the superscript $*$ denotes complex conjugation. The subscript $S = 2$ has been omitted for brevity. It should be noted that the angular functions of Eq. (5) differ by a factor of $\zeta = (-1)^{L_A - L_B} (4\pi)^{-3/2} (2L_{AB} + 1) [(2L_A + 1)(2L_B + 1)]^{1/2}$ from the functions used in Ref. [28], i.e. the $v_{L_A, L_B, L_{AB}}(R)$ expansion coefficients of Ref. [28] must be multiplied by ζ to obtain the potential in the form of Eq. (4).

In the absence of an external field, both the total angular momentum \mathcal{J} and its space-fixed projection \mathcal{M} are rigorously conserved. We therefore expand the wave function in a

total angular momentum basis:

$$\begin{aligned} \Psi^{\mathcal{J},\mathcal{M}}(R, \Omega, \omega_A, \omega_B, \sigma_A, \sigma_B) &= \frac{1}{R} \sum_{N_A, N_B, N, S_A, S_B, S, J, L} \chi_{N_A, N_B, N, S_A, S_B, S, J, L}^{\mathcal{J}, \mathcal{M}}(R) \\ &\times \psi_{N_A, N_B, N, S_A, S_B, S, J, L}^{\mathcal{J}, \mathcal{M}}(\Omega, \omega_A, \omega_B, \sigma_A, \sigma_B), \end{aligned} \quad (6)$$

where σ_A and σ_B refer to the electronic spin coordinates of molecules A and B , respectively. Here N_A and N_B denote the rotational quantum numbers of the two monomers, N is the coupled rotational quantum number of the complex, S_A and S_B are the monomer spin quantum numbers, which are coupled into total spin S , J is the angular momentum quantum number arising from the coupling of N and S , and L denotes the partial-wave angular momentum. The coupled angular momentum basis functions are defined as follows:

$$\begin{aligned} \psi_{N_A, N_B, N, S_A, S_B, S, J, L}^{\mathcal{J}, \mathcal{M}}(\Omega, \omega_A, \omega_B, \sigma_A, \sigma_B) &= \\ &\sum_{M_J, M_L} \sum_{M_N, M_S} \sum_{M_{S_A}, M_{S_B}} \sum_{M_{N_A}, M_{N_B}} Y_{N_A, M_{N_A}}(\omega_A) Y_{N_B, M_{N_B}}(\omega_B) Y_{L, M_L}(\Omega) \\ &\times \tau_{S_A, M_{S_A}}(\sigma_A) \tau_{S_B, M_{S_B}}(\sigma_B) \langle N_A M_{N_A} N_B M_{N_B} | N M_N \rangle \langle S_A M_{S_A} S_B M_{S_B} | S M_S \rangle \\ &\times \langle N M_N S M_S | J M_J \rangle \langle J M_J L M_L | \mathcal{J} \mathcal{M} \rangle, \end{aligned} \quad (7)$$

where $\tau_{S_A, M_{S_A}}$ and $\tau_{S_B, M_{S_B}}$ are spinor wave functions. Here the quantum numbers M_{N_i} , M_{S_i} , M_N , M_S , M_J , and M_L denote the projections of N_i , S_i , N , S , J , and L onto the magnetic-field axis. We will restrict the basis such that N_A and N_B range from 0 to N_{\max} and $L = 0, \dots, L_{\max}$. Note that the scattering calculations in this basis may also be performed for a single dimer spin state S . As detailed in Section III B, we will exploit this feature to investigate the validity of describing all three dimer spin states by the $S = 2$ potential energy surface.

Since target and projectile are identical, we can symmetrize the wave function with respect to the permutation operator \hat{P}_{AB} . This yields the following normalized basis functions:

$$\begin{aligned} \phi_{N_A, N_B, N, S_A, S_B, S, J, L}^{\eta, \mathcal{J}, \mathcal{M}} &= \frac{1}{[2(1 + \delta_{N_A N_B} \delta_{S_A S_B})]^{1/2}} [\psi_{N_A, N_B, N, S_A, S_B, S, J, L}^{\mathcal{J}, \mathcal{M}} \\ &+ \eta(-1)^{L+N_A+N_B-N+S_A+S_B-S} \psi_{N_B, N_A, N, S_B, S_A, S, J, L}^{\mathcal{J}, \mathcal{M}}]. \end{aligned} \quad (8)$$

Here $\eta = +1$ corresponds to composite bosons and $\eta = -1$ to composite fermions, assuming that the molecules are in their nuclear-spin stretched states. To obtain a linearly independent basis, the index pair (N_A, N_B) must be restricted such that $N_A \geq N_B$ [37]. Finally, the

basis functions of Eq. (8) are also eigenfunctions of the inversion operator, with eigenvalues $\epsilon = (-1)^{N_A+N_B+L}$. Thus, the Hamiltonian in the symmetry-adapted basis consists of four blocks, each block labeled by η and the parity ϵ . It must be noted, however, that the wave function of Eq. (8) vanishes for $(\eta = +1, \epsilon = -1)$ and $(\eta = -1, \epsilon = +1)$ if the molecules are in the magnetically trapped ground state with $N_A = N_B = N = 0$ and $S = 2$. We therefore only need to consider the parity case $\epsilon = +1$ for $\eta = +1$ and $\epsilon = -1$ for $\eta = -1$.

The matrix elements of the Hamiltonian in the symmetry-adapted basis [Eq. (8)] can be readily obtained from the matrix elements in the ‘primitive’ basis $\psi_{N_A, N_B, N, S_A, S_B, S, J, L}^{\mathcal{J}, \mathcal{M}}$. These are given in the Appendix.

B. S -matrices and cross sections

The close-coupling equations are solved for each \mathcal{J} and each symmetry type (η, ϵ) using the hybrid log-derivative method of Alexander and Manolopoulos [38]. This algorithm uses a fixed-step-size log-derivative propagator in the short range and a variable-step-size Airy propagator in the long range. The solutions are then matched to asymptotic boundary conditions to obtain the scattering S -matrices. Since we consider only the field-free case, the results are independent of the total angular momentum projection \mathcal{M} .

Although we assume zero magnetic field in our calculations, we are ultimately interested in the elastic and inelastic spin-changing cross sections for magnetically trapped NH. It is therefore necessary to transform the S -matrices to a channel product eigenbasis of the form $|(\bar{N}_A, S_A)J_A, M_{J_A}\rangle|(\bar{N}_B, S_B)J_B, M_{J_B}\rangle|L, M_L\rangle$, where J_i and M_{J_i} arise from the angular momentum coupling of \bar{N}_i and S_i . Here we have used the notation \bar{N}_i instead of N_i , because N_i is strictly not a good quantum number. This is due to the intramolecular spin-spin coupling, which mixes states with N_i and $N_i \pm 2$. However, the mixing is quite weak and \bar{N}_i corresponds almost exactly to N_i . A symmetry-adapted version of the channel eigenbasis is given by

$$\begin{aligned} \phi_{\bar{N}_A, S_A, J_A, M_{J_A}, \bar{N}_B, S_B, J_B, M_{J_B}, L, M_L}^\eta &= \frac{1}{[2(1 + \delta_{\bar{N}_A \bar{N}_B} \delta_{S_A S_B} \delta_{J_A J_B} \delta_{M_{J_A} M_{J_B}})]^{1/2}} \\ &\times [|(\bar{N}_A, S_A)J_A, M_{J_A}\rangle|(\bar{N}_B, S_B)J_B, M_{J_B}\rangle|L, M_L\rangle \\ &\times +\eta(-1)^L |(\bar{N}_B, S_B)J_B, M_{J_B}\rangle|(\bar{N}_A, S_A)J_A, M_{J_A}\rangle|L, M_L\rangle]. \end{aligned} \quad (9)$$

It should be noted that the total angular momentum \mathcal{J} is not a good quantum number here,

but its laboratory-frame projection $\mathcal{M} = M_{J_A} + M_{J_B} + M_L$ is conserved.

The basis transformation from Eq. (8) to Eq. (9) cannot be performed analytically, because N_i , N , and S are only approximately good quantum numbers. We have therefore developed a numerical scheme in which the channel eigenfunctions of Eq. (9) are obtained as the simultaneous eigenvectors of the operators $\{\hat{L}^2, \hat{H}_A + \hat{H}_B, \hat{J}_{z_A} + \hat{J}_{z_B}, \hat{J}_{z_A}^2 + \hat{J}_{z_B}^2\}$. Note that these operators all commute with each other and with \hat{P}_{AB} . The numerical procedure works as follows. We start by diagonalizing the first operator, e.g. the matrix representation of the \hat{L}^2 operator, constructed in the basis of Eq. (8). In each degenerate subspace of \hat{L}^2 , we set up the matrix of the next operator and diagonalize it. This process is repeated for the remaining operators until all eigenvectors are unique. We note that the operator $\hat{J}_{z_A}^2 + \hat{J}_{z_B}^2$ is only required to distinguish between states with coincidental degeneracies in $M_{J_A} + M_{J_B}$, e.g. the states $|\phi_{0,1,1,0,0,1,1,0,0,0}^\eta\rangle$ with $M_{J_A} = M_{J_B} = 0$ and $|\phi_{0,1,1,1,0,1,1,-1,0,0}^\eta\rangle$ with $M_{J_A} = 1, M_{J_B} = -1$. Any remaining degeneracies arising from $\hat{H}_A + \hat{H}_B$ may be lifted by diagonalizing the operator $\hat{H}_A^2 + \hat{H}_B^2$, but such degeneracies occur only for higher energies. In the cold and ultracold regime, these higher-energy channels are closed and the eigenvalues of \hat{L}^2 , $\hat{H}_A + \hat{H}_B$, $\hat{J}_{z_A} + \hat{J}_{z_B}$, and $\hat{J}_{z_A}^2 + \hat{J}_{z_B}^2$ are sufficient to uniquely identify all relevant quantum numbers. It must be noted that, since \hat{J}_{z_A} and \hat{J}_{z_B} do not separately commute with \hat{P}_{AB} , the matrices of $\hat{J}_{z_A} + \hat{J}_{z_B}$ and $\hat{J}_{z_A}^2 + \hat{J}_{z_B}^2$ are not trivially constructed in the basis of Eq. (8). We obtained these matrices by first evaluating the \hat{J}_{z_i} and $\hat{J}_{z_i}^2$ operators in a fully decoupled basis of the form $|N_A, M_{N_A}, S_A, M_{S_A}, N_B, M_{N_B}, S_B, M_{S_B}, L, M_L\rangle$. Both \hat{J}_{z_i} and $\hat{J}_{z_i}^2$ are diagonal in this basis, with diagonal elements $M_{J_i} = M_{N_i} + M_{S_i}$ and $M_{J_i}^2$, respectively. We subsequently performed an analytical transformation to the coupled basis of Eq. (7) using the appropriate Clebsch-Gordan coefficients. Finally, we used a rectangular transformation matrix for $\hat{J}_{z_A} + \hat{J}_{z_B}$ and $\hat{J}_{z_A}^2 + \hat{J}_{z_B}^2$ to account for the symmetry adaptation, i.e. to transform the matrices to the basis of Eq. (8).

The evaporative cooling rate for cold magnetically trapped NH molecules, with quantum numbers $\bar{N}_A = \bar{N}_B = 0$, $J_A = J_B = 1$, and $M_{J_A} = M_{J_B} = 1$, is determined by the ratio between elastic and M_J -changing cross sections. The cross-section expression for indistinguishable molecules at total energy E is [30]

$$\sigma_{\gamma_A \gamma_B \rightarrow \gamma'_A \gamma'_B}^\eta(E) = \frac{\pi(1 + \delta_{\gamma_A \gamma_B})}{k_{\gamma_A \gamma_B}^2} \sum_{L, M_L} \sum_{L', M'_L} \left| T_{\gamma_A \gamma_B L M_L; \gamma'_A \gamma'_B L' M'_L}^\eta(E) \right|^2, \quad (10)$$

where we have introduced the shorthand notation $\gamma_A \gamma_B$ to label the symmetrized monomer

states, i.e. $\phi_{\bar{N}_A, S_A, J_A, M_{J_A}, \bar{N}_B, S_B, J_B, M_{J_B}, L, M_L}^\eta \equiv |\gamma_A \gamma_B\rangle |LM_L\rangle$, and $k_{\gamma_A \gamma_B}$ is the length of the wavevector for the initial collision channel $|\gamma_A \gamma_B\rangle$. The T -matrix elements are defined in terms of the transformed S -matrix elements as $T_{\gamma_A \gamma_B LM_L; \gamma'_A \gamma'_B L' M'_L}^\eta = \delta_{\gamma_A \gamma'_A} \delta_{\gamma_B \gamma'_B} \delta_{LL'} \delta_{M_L M'_L} - S_{\gamma_A \gamma_B LM_L; \gamma'_A \gamma'_B L' M'_L}^\eta$. Finally, we note that the summations over M_L and M'_L in Eq. (10) may also be understood as a sum over all possible \mathcal{M} values, since $\mathcal{M} = M_{J_A} + M_{J_B} + M_L = M'_{J_A} + M'_{J_B} + M'_L$.

C. Computational details

The scattering calculations were performed using a modified version of the MOLSCAT package [39, 40] in which the coupled basis set of Eq. (6) was implemented. The radial grid ranged from 4.5 to 500 a_0 , with the Airy propagation starting at 15 a_0 . The step size for the log-derivative propagator was 0.02 a_0 . The basis set included all functions up to $N_A = N_B = 5$ and $L = 6$. The expansion of the quintet potential was truncated at $L_A = L_B = 6$. As mentioned in Section II A, the chemically reactive singlet and triplet interaction potentials were excluded from the calculations, and were replaced by the nonreactive $S = 2$ surface. Thus, we assumed that all three spin states are described by the same potential energy surface. In order to study the role of the $S = 0$ and 1 states under this assumption, we also performed scattering calculations for the quintet state only.

At each collision energy, the scattering S -matrices were accumulated for all relevant \mathcal{J} values and subsequently transformed to the channel eigenbasis of Eq. (9) for all possible \mathcal{M} values. The basis transformation was carried out in Matlab [41]. The total elastic and inelastic cross sections were then obtained using Eq. (10).

III. RESULTS AND DISCUSSION

A. Cross sections

The elastic and M_J -changing cross sections for magnetically trapped ^{14}NH and ^{15}NH are shown in Fig. 1. At low collision energies, the cross sections are dominated by incoming s -waves for bosonic ^{15}NH and by p -waves for fermionic ^{14}NH . The observed energy dependence

is consistent with Wigner's threshold law for iso-energetic processes [42, 43]:

$$\sigma \propto E^{L+L'}, \quad (11)$$

where L and L' denote the partial waves in the incoming and outgoing channels, respectively. For elastic $^{15}\text{NH} + ^{15}\text{NH}$ collisions, we have $L = L' = 0$ and the cross section is constant as a function of E . For inelastic collisions, the change in M_{J_A} or M_{J_B} must be accompanied by a change in the M_L quantum number, which follows from the conservation of \mathcal{M} . Since the parity $(-1)^{N_A+N_B+L}$ is also rigorously conserved, it is easily verified [see Eq. (8)] that the dominant inelastic cross section for ^{15}NH ($L = 0$) corresponds to the $L' = 2$ outgoing channel, and consequently behaves as E^2 . For fermionic $^{14}\text{NH} + ^{14}\text{NH}$ collisions, both the elastic and inelastic channels are dominated by $L = L' = 1$ [see Eq. (8)], yielding the observed E^2 behaviour. We also point out that, in the presence of a magnetic field, all inelastic transitions would be exothermic and the corresponding cross section would behave as $E^{L-1/2}$ [42]. This leads to a different elastic-to-inelastic collision ratio than in the field-free case. It is shown in a separate publication that the ratio for $^{15}\text{NH} + ^{15}\text{NH}$ collisions is still very favorable when the magnetic field is explicitly included [34].

We find that ^{15}NH is more suitable for evaporative cooling than ^{14}NH , in agreement with the findings of Kajita [33]. More specifically, we see in Fig. 1 that the elastic-to-inelastic ratio for $^{15}\text{NH} + ^{15}\text{NH}$ far exceeds the critical value of 150 for all energies below $E \approx 10^{-2}$ K, while for $^{14}\text{NH} + ^{14}\text{NH}$ the ratio is orders of magnitude smaller and is close to unity at collision energies below 10^{-4} K. This result is essentially a consequence of the Pauli principle, which forbids s -wave scattering for $^{14}\text{NH} + ^{14}\text{NH}$. We emphasize that our calculations were performed under the assumption that both molecules are in their nuclear-spin stretched states, giving rise to a symmetric nuclear-spin wave function. This leads to the restriction that $\eta = +1$ ($\epsilon = +1$) for ^{15}NH and $\eta = -1$ ($\epsilon = -1$) for ^{14}NH . If, however, the two monomers were in *different* nuclear-spin states, the corresponding wave function may also be antisymmetric under exchange and both values of η would be allowed. In that case, the total cross section is given by a weighted sum over the cross sections σ^{+1} and σ^{-1} :

$$\sigma_{\gamma_A\gamma_B \rightarrow \gamma'_A\gamma'_B}(E) = W^+ \sigma_{\gamma_A\gamma_B \rightarrow \gamma'_A\gamma'_B}^{+1}(E) + W^- \sigma_{\gamma_A\gamma_B \rightarrow \gamma'_A\gamma'_B}^{-1}(E), \quad (12)$$

with W^+ and W^- denoting the relative spin-statistical weights. The weights are $W^+ = 5/12$ and $W^- = 7/12$ for fermionic ^{14}NH and $3/4$ and $1/4$ for bosonic ^{15}NH . Figure 2 shows the

results for $^{14}\text{NH} - ^{14}\text{NH}$, assuming a mixture of different nuclear-spin states. The inclusion of even- L partial waves ($\eta = +1$) strongly enhances the efficiency of evaporative cooling for ^{14}NH , in particular due to the s -wave elastic contribution. For $^{15}\text{NH} - ^{15}\text{NH}$, the addition of odd- L partial wave contributions ($\eta = -1$) will probably lead to a slightly lower elastic-to-inelastic ratio. This is because the odd- L elastic cross section, which vanishes as E^2 , is almost negligible compared to the s -wave elastic cross section in the ultracold limit. The odd- L inelastic contribution, on the other hand, exhibits the same threshold behaviour as the even- L inelastic cross section, and could easily increase the total inelastic loss by a factor of ~ 2 . Hence we conclude that, in order to achieve efficient evaporative cooling, bosonic ^{15}NH should be prepared in a single nuclear-spin state, while for ^{14}NH the molecules should be in a mixture of hyperfine states.

Aside from symmetry arguments, the difference between $^{15}\text{NH} - ^{15}\text{NH}$ and $^{14}\text{NH} - ^{14}\text{NH}$ is relatively small. The rotational and spin-rotation constants differ by only 0.45% and the reduced masses of the collision complex are 6.6% different. Since ^{15}NH is more advantageous for evaporative cooling, we will only consider collisions between ^{15}NH molecules in the remainder of this work. Again it will be assumed that the monomers are in identical hyperfine states, so that only the $\eta = +1$ ($\epsilon = +1$) symmetry case needs to be examined.

State-to-state inelastic cross sections for magnetically trapped ^{15}NH ($M_{J_A} = 1, M_{J_B} = 1$) are shown in Fig. 3. We find that transitions to the states with $|M_{J_A} = 1, M_{J_B} = 0\rangle$, $|M_{J_A} = 1, M_{J_B} = -1\rangle$, and $|M_{J_A} = 0, M_{J_B} = 0\rangle$ are dominant in the ultracold regime. It can also be seen that these cross sections follow an E^2 dependence below $\sim 10^{-4}$ K. The inelastic cross sections for $|M_{J_A} = 0, M_{J_B} = -1\rangle$ and $|M_{J_A} = -1, M_{J_B} = -1\rangle$ exhibit E^4 behaviour at low collision energies. These results are consistent with the threshold laws of Krems and Dalgarno for collisional reorientation of angular momentum in the absence of an external field [43]. Although these laws were derived for collisions of paramagnetic species with structureless targets, they also apply to $^{15}\text{NH} + ^{15}\text{NH}$ collisions:

$$\sigma_{J,M_J \rightarrow J,M_J \pm \Delta M_J} \propto E^{\Delta M_J} \quad (13)$$

if ΔM_J is even and

$$\sigma_{J,M_J \rightarrow J,M_J \pm \Delta M_J} \propto E^{\Delta M_J + 1} \quad (14)$$

if ΔM_J is odd. Here ΔM_J is defined as the change in $M_{J_A} + M_{J_B}$. It also follows from Eq. (13) that the elastic cross section ($\Delta M_J = 0$) is constant at low energies, in agreement with

Eq. (11).

B. Contributions from singlet and triplet states

Throughout this paper, we have assumed that all three spin states of the NH–NH complex are described by a single nonreactive potential-energy surface, namely the $S = 2$ surface. The $S = 2$ state corresponds to the case where both monomers are magnetically trapped, and is therefore the most relevant spin state in our present study. It is, however, not *a priori* clear how the $S = 0$ and 1 states can influence the trap loss probability, and how well they can be described by the quintet surface.

We must first point out that, even at infinite separation, S is strictly not a good quantum number due to the intramolecular spin-spin coupling. However, the coupling between different spin states is relatively weak and we may therefore treat S as nearly exact. Specifically, for the rotational ground state of the complex, the initial state with $M_{J_A} = M_{J_B} = 1$ corresponds almost exclusively (99.98%) to the quintet state.

In order to investigate the contributions from the $S = 0$ and 1 states, we have performed scattering calculations with all singlet and triplet functions removed from the basis set. The results are shown in Fig. 4 as a function of energy. The cross sections for the full basis set, i.e. with all three spin states included, are also plotted for comparison. It can be seen that exclusion of the $S = 0$ and 1 states has a rather small effect on the cross section, suggesting that most of the trap loss takes place within the quintet state. Thus, the singlet and triplet states play a minor role in the collision dynamics when described by the nonreactive $S = 2$ potential.

If the $S = 0$ and 1 states would be described by their true, reactive surfaces, it can be expected that any transition to the singlet or triplet state leads to chemical reaction and consequent trap loss. In that case, however, the potentials are no longer degenerate at short range and the probability for hopping from the quintet surface to another state is most probably *decreased* due to the energy gap law. That is, inclusion of the reactive $S = 0$ and 1 surfaces will probably not lead to a larger inelastic cross section, and our assumption of including only the nonreactive $S = 2$ surface is very reasonable. In this respect, we may also view the M_J -changing cross sections presented in Fig. 4 as approximate upper bounds. Nevertheless, it must be noted that the relatively deep wells in the reactive potentials will

give rise to a large number of bound states, which in turn may cause strong resonances in the cross sections. In order to verify these assumptions, we plan to perform reactive quantum scattering calculations for $\text{NH} + \text{NH}$ with all three interaction potentials included.

C. Sensitivity to potential and basis-set size

In this section we address two interrelated topics, namely the sensitivity to the potential and the dependence on the angular basis-set size. It is well established that low-energy scattering depends strongly on the presence of bound and quasi-bound states near the dissociation threshold. Such states can give rise to scattering resonances that may enhance the collision cross section by several orders of magnitude. The energies of these (quasi-)bound states are highly sensitive to the details of the potential-energy surface, and hence they are very difficult to predict from first principles. Even a state-of-the-art *ab initio* potential cannot reliably predict whether a particular near-dissociation state lies above or below the threshold. This is particularly true for systems with multiple degrees of freedom and deep potential wells, for which the density of states is relatively high. Thus, in order to assess the accuracy of the cross sections, we must carefully take into account the effect of uncertainties in the potential. In a related manner, we also consider the effect of using different channel basis-set sizes in the scattering calculations. The size of the angular basis set can influence the energies of the (quasi-)bound states, which in turn can lead to a different resonance structure. It will be demonstrated, however, that the use of a reduced basis set leads only to a shift in the resonance positions, and does not significantly alter the general resonance pattern.

We first consider the sensitivity of the calculated cross sections to the potential-energy surface. Our potential has been obtained from state-of-the-art *ab initio* calculations, and we estimate that it differs from the exact potential by at most a few percent. For practical reasons, we have studied the potential dependence indirectly by performing scattering calculations as a function of the reduced mass μ . Since scaling the reduced mass by a factor of λ ($\mu_{\text{scaled}} = \lambda\mu$) is almost equivalent to scaling the entire interaction potential by λ [24], this provides a stringent test for the sensitivity to the potential. The true potential does not necessarily differ from our *ab initio* surface by only a constant factor, but scaling by λ ($0.9 \leq \lambda \leq 1.1$) amply samples the range of possibilities within which the exact potential is

expected to lie.

Figure 5 shows the cross sections as a function of λ at collision energies of 10^{-6} K, 10^{-4} K, and 10^{-3} K. It can be seen that both the elastic and inelastic cross sections change by several orders of magnitude as a function of λ , but they vary about a certain background value. For instance, the elastic cross sections fluctuate around $\sim 10^{-12}$ cm² for all three collision energies. The background values for the inelastic cross sections increase with E^2 in the ultracold regime, consistent with the results of Fig. 1 and the threshold laws discussed in Sec. III A. The deviations from the background values are due to scattering resonances, which arise from NH–NH states that change from bound to quasi-bound at the $|M_{J_A} = 1, M_{J_B} = 1\rangle$ threshold. Such resonance features are to be expected as a function of λ , since a scaling of the potential, or in fact any modification of the potential-energy surface, will cause a shift in the bound-state energies. For 10^{-6} , 10^{-4} K, and 10^{-3} K, the resonances are located around the same values of λ , and hence the λ -dependent resonance structure would not be averaged out in a thermal (Maxwell-Boltzmann) distribution at temperatures below 1 mK. That is, thermally averaged rate constants are likely to show a similar sensitivity to the potential as the calculated cross sections.

Let us now consider the elastic-to-inelastic cross-section ratios as a function of λ . These are shown in Fig. 6 for $E = 10^{-6}$ K, 10^{-4} K, and 10^{-3} K. For clarity, we have also indicated the critical ratio of 150 that is required for efficient evaporative cooling. As can be seen, the calculated ratios exceed 150 for almost all values of λ and all energies considered, except when λ is close to resonance. This demonstrates that evaporative cooling of NH is feasible at energies below 1 mK for most of the λ -values considered. Although we cannot predict which value of λ corresponds most closely to the exact potential, we do expect that the sampled range of λ is indicative of the range within which the exact potential lies, and hence we conclude that the *probability* for successful evaporative cooling is relatively large. That is, the true potential is very likely to be such that the elastic-to-inelastic ratio exceeds 150.

The λ -scaling approach is also used to investigate the influence of the angular basis-set size on the scattering results. First we point out that the strong anisotropy of the potential and the large reduced mass of NH–NH require relatively high values of the basis-set parameters N_{\max} and L_{\max} . In addition, the triplet spins on the monomers increase the channel basis-set size by a factor of 9, making it highly challenging to achieve full basis-set convergence. Figure 7 shows the cross sections as a function of λ for different values of N_{\max} and L_{\max} at

a collision energy of 10^{-6} K. The maximum number of channels in these calculations ranged from 937 for $N_{\text{max}} = 4$ and $L_{\text{max}} = 6$ ($\mathcal{J} = 4$) up to 2382 for $N_{\text{max}} = 6$ and $L_{\text{max}} = 6$ ($\mathcal{J} = 5$). It can be seen that the cross sections all vary by several orders of magnitude as a function of λ , and for a given value of λ the four basis sets can yield very different numerical results. However, the different cross sections vary about the same background values and the resonant features have similar widths for all four basis sets. Thus, a change in N_{max} or L_{max} may cause a shift in the positions of the resonances, but the overall pattern is virtually unaffected. The estimated probability for successful evaporative cooling, i.e. the probability that the exact potential is such that the elastic-to-inelastic cross-section ratio exceeds 150, is therefore similar for all four basis sets. This can also be understood by considering that a change in the basis set only shifts the bound-state energy levels, similar to the effect of scaling the potential.

The results of Fig. 7 demonstrate that the cross sections are almost, but not fully converged with respect to N_{max} and L_{max} . Using a larger basis set is infeasible at present given the available computer power. A larger basis set would also require additional terms in the expansion of the potential anisotropy [Eq. (4)], making the calculation prohibitively expensive. Moreover, taking into account the uncertainty in the potential, even a fully converged basis set would not give really reliable numerical values due to the presence of (quasi-)bound state resonances. Since the exact form of the potential, and thus the precise locations of the resonances, are still unknown, the calculated cross sections are subject to an inherent degree of uncertainty that cannot be reduced by the use of a fully converged basis set. In this sense, full basis-set convergence will not necessarily yield a more accurate prediction of the true cross sections. On the other hand, the *probability* for successful evaporative cooling can be reliably predicted using an incompletely converged basis set, and hence we conclude that, even if full basis-set convergence could be achieved, this would not significantly alter our main qualitative results. We emphasize, however, that it is crucial to test the sensitivity to the potential in order to assess the accuracy of the calculated cross sections. As a final point, we note that the uncertainty limits of the potential could, in principle, be greatly reduced by measuring the cross sections experimentally.

IV. CONCLUSIONS

We have carried out elastic and inelastic quantum scattering calculations on a state-of-the-art *ab initio* potential to study field-free NH + NH collisions at low and ultralow temperatures. The results indicate that, when the molecules are prepared in their nuclear spin-stretched states, bosonic ^{15}NH is more suitable for evaporative cooling than fermionic ^{14}NH . This is a direct consequence of the Pauli principle, which forbids *s*-wave scattering for two identical fermions. The ^{14}NH isotope may also be successfully cooled, however, when the monomers are in a mixture of different nuclear spin states.

We have assumed that all three spin states of the NH–NH complex are described by the nonreactive quintet surface. This approximation is shown to be reasonable, although a full reactive scattering calculation would be required to investigate the precise role of the chemically active singlet and triplet states.

The collision cross sections are sensitive to the details of the interaction potential, because of the presence of quasi-bound states that cause scattering resonances. Since the exact interaction potential is unknown, this gives rise to a degree of uncertainty in the numerical cross sections. However, a sampling of the range of possibilities indicates that the exact potential is very likely to be such that the elastic-to-inelastic cross-section ratio is favorable for evaporative cooling. This result is only weakly dependent on the size of the channel basis set. In particular, the effect of using a reduced basis set is very similar to a scaling of the potential within its uncertainty. We conclude that even without full basis-set convergence, which is extremely difficult to achieve for systems such as NH–NH, we can provide valuable insight into the feasibility of evaporative cooling. This also offers hope for the theoretical treatment of other challenging open-shell molecule + molecule systems.

Acknowledgments

We gratefully acknowledge EPSRC for funding the collaborative project CoPoMol under the ESF EUROCORES programme EuroQUAM. LMCJ and GCG thank the Council for Chemical Sciences of the Netherlands Organization for Scientific Research (CW-NWO) for financial support.

Appendix: Matrix elements

In this Appendix, we present the matrix elements of the scattering Hamiltonian in the ‘primitive’ basis $\psi_{N_A, N_B, N, S_A, S_B, S, J, L}^{\mathcal{J}, \mathcal{M}}$. The matrix elements in the symmetry-adapted basis can be obtained using Eq. (8). For the angular functions of the potential we have

$$\begin{aligned}
& \langle \psi_{N_A, N_B, N, S_A, S_B, S, J, L}^{\mathcal{J}, \mathcal{M}} | A_{L_A, L_B, L_{AB}} | \psi_{N'_A, N'_B, N', S_A, S_B, S', J', L'}^{\mathcal{J}, \mathcal{M}} \rangle = \\
& \delta_{SS'} \left(\frac{1}{4\pi} \right)^{3/2} (-1)^{N_A + N_B + N + S + L_{AB} + \mathcal{J}} \\
& \times [L_{AB}] \sqrt{[L_A][L_B][N_A][N'_A][N_B][N'_B][N][N'][L][L'][J][J']} \\
& \times \begin{pmatrix} N_A & L_A & N'_A \\ 0 & 0 & 0 \end{pmatrix} \begin{pmatrix} N_B & L_B & N'_B \\ 0 & 0 & 0 \end{pmatrix} \begin{pmatrix} L & L_{AB} & L' \\ 0 & 0 & 0 \end{pmatrix} \\
& \times \begin{Bmatrix} J & J' & L_{AB} \\ L' & L & \mathcal{J} \end{Bmatrix} \begin{Bmatrix} N' & N & L_{AB} \\ J & J' & S \end{Bmatrix} \begin{Bmatrix} N_A & N'_A & L_A \\ N_B & N'_B & L_B \\ N & N' & L_{AB} \end{Bmatrix}, \tag{A.1}
\end{aligned}$$

with the factors in large round brackets denoting Wigner $3j$ symbols, the factors in curly brackets denoting $6j$ and $9j$ symbols, and $[Q] = (2Q + 1)$. The intermolecular magnetic dipole term is given by:

$$\begin{aligned}
& \langle \psi_{N_A, N_B, N, S_A, S_B, S, J, L}^{\mathcal{J}, \mathcal{M}} | V_{\text{magn.dip}} | \psi_{N'_A, N'_B, N', S_A, S_B, S', J', L'}^{\mathcal{J}, \mathcal{M}} \rangle = \\
& - \delta_{N_A N'_A} \delta_{N_B N'_B} \delta_{N N'} \sqrt{30} g_S^2 \mu_B^2 \frac{\alpha^2}{R^3} (-1)^{N + S' + J + J' + \mathcal{J}} \\
& \times \sqrt{S_A(S_A + 1)S_B(S_B + 1)[S_A][S_B][S][S'][J][J'][L][L']} \\
& \times \begin{pmatrix} L & 2 & L' \\ 0 & 0 & 0 \end{pmatrix} \begin{Bmatrix} J & J' & 2 \\ L' & L & \mathcal{J} \end{Bmatrix} \begin{Bmatrix} J' & J & 2 \\ S & S' & N \end{Bmatrix} \begin{Bmatrix} S_A & S_A & 1 \\ S_B & S_B & 1 \\ S & S' & 2 \end{Bmatrix}. \tag{A.2}
\end{aligned}$$

The rotation operators for the two monomers ($i = A, B$) are completely diagonal in the angular basis:

$$\begin{aligned}
& \langle \psi_{N_A, N_B, N, S_A, S_B, S, J, L}^{\mathcal{J}, \mathcal{M}} | B_0 \hat{N}_i^2 | \psi_{N'_A, N'_B, N', S_A, S_B, S', J', L'}^{\mathcal{J}, \mathcal{M}} \rangle = \\
& \delta_{N_A N'_A} \delta_{N_B N'_B} \delta_{N N'} \delta_{SS'} \delta_{JJ'} \delta_{LL'} B_0 N_i(N_i + 1). \tag{A.3}
\end{aligned}$$

For the spin-rotation coupling terms we find

$$\begin{aligned}
& \langle \psi_{N_A, N_B, N, S_A, S_B, S, J, L}^{\mathcal{J}, \mathcal{M}} | \gamma \hat{\mathbf{N}}_A \cdot \hat{\mathbf{S}}_A | \psi_{N'_A, N'_B, N', S_A, S_B, S', J', L'}^{\mathcal{J}, \mathcal{M}} \rangle = \\
& \delta_{N_A N'_A} \delta_{N_B N'_B} \delta_{JJ'} \delta_{LL'} \gamma (-1)^{N_A + N_B + S_A + S_B + S + S' + J} \\
& \times \sqrt{N_A(N_A + 1) S_A(S_A + 1) [N_A][S_A][N][N'][S][S']} \\
& \times \begin{Bmatrix} N_A & N_A & 1 \\ N & N' & N_B \end{Bmatrix} \begin{Bmatrix} S_A & S_A & 1 \\ S & S' & S_B \end{Bmatrix} \begin{Bmatrix} N & N' & 1 \\ S' & S & J \end{Bmatrix}, \tag{A.4}
\end{aligned}$$

$$\begin{aligned}
& \langle \psi_{N_A, N_B, N, S_A, S_B, S, J, L}^{\mathcal{J}, \mathcal{M}} | \gamma \hat{\mathbf{N}}_B \cdot \hat{\mathbf{S}}_B | \psi_{N'_A, N'_B, N', S_A, S_B, S', J', L'}^{\mathcal{J}, \mathcal{M}} \rangle = \\
& \delta_{N_A N'_A} \delta_{N_B N'_B} \delta_{JJ'} \delta_{LL'} \gamma (-1)^{N_A + N_B + N + N' S_A + S_B + J} \\
& \times \sqrt{N_B(N_B + 1) S_B(S_B + 1) [N_B][S_B][N][N'][S][S']} \\
& \times \begin{Bmatrix} N' & N & 1 \\ N_B & N_B & N_A \end{Bmatrix} \begin{Bmatrix} S' & S & 1 \\ S_B & S_B & S_A \end{Bmatrix} \begin{Bmatrix} N & N' & 1 \\ S' & S & J \end{Bmatrix}, \tag{A.5}
\end{aligned}$$

and, finally, for the intramolecular spin-spin operators $\hat{V}_{\text{SS}}^{(i)}$ we have

$$\begin{aligned}
& \langle \psi_{N_A, N_B, N, S_A, S_B, S, J, L}^{\mathcal{J}, \mathcal{M}} | \hat{V}_{\text{SS}}^{(A)} | \psi_{N'_A, N'_B, N', S_A, S_B, S', J', L'}^{\mathcal{J}, \mathcal{M}} \rangle = \\
& \delta_{N_B N'_B} \delta_{JJ'} \delta_{LL'} \frac{2}{3} \sqrt{30} \lambda_{\text{SS}} (-1)^{N_B + S_A + S_B + S + S' + J} \\
& \times S_A(S_A + 1)(2S_A + 1) \sqrt{[N_A][N'_A][N][N'][S][S']} \begin{pmatrix} N_A & 2 & N'_A \\ 0 & 0 & 0 \end{pmatrix} \\
& \times \begin{Bmatrix} N'_A & N_A & 2 \\ N & N' & N_B \end{Bmatrix} \begin{Bmatrix} S_A & S_A & 1 \\ 1 & 2 & S_A \end{Bmatrix} \begin{Bmatrix} S_A & S_A & 2 \\ S & S' & S_B \end{Bmatrix} \begin{Bmatrix} N & N' & 2 \\ S' & S & J \end{Bmatrix}, \tag{A.6}
\end{aligned}$$

$$\begin{aligned}
& \langle \psi_{N_A, N_B, N, S_A, S_B, S, J, L}^{\mathcal{J}, \mathcal{M}} | \hat{V}_{\text{SS}}^{(B)} | \psi_{N'_A, N'_B, N', S_A, S_B, S', J', L'}^{\mathcal{J}, \mathcal{M}} \rangle = \\
& \delta_{N_A N'_A} \delta_{JJ'} \delta_{LL'} \frac{2}{3} \sqrt{30} \lambda_{\text{SS}} (-1)^{N_A + N_B + N'_B + N + N' + S_A + S_B + J} \\
& \times S_B(S_B + 1)(2S_B + 1) \sqrt{[N_B][N'_B][N][N'][S][S']} \begin{pmatrix} N_B & 2 & N'_B \\ 0 & 0 & 0 \end{pmatrix} \\
& \times \begin{Bmatrix} N' & N & 2 \\ N_B & N'_B & N_A \end{Bmatrix} \begin{Bmatrix} S_B & S_B & 1 \\ 1 & 2 & S_B \end{Bmatrix} \begin{Bmatrix} S' & S & 2 \\ S_B & S_B & S_A \end{Bmatrix} \begin{Bmatrix} N & N' & 2 \\ S' & S & J \end{Bmatrix}. \tag{A.7}
\end{aligned}$$

[1] A. Micheli, G. K. Brennen, and P. Zoller, Nat. Phys. **2**, 341 (2006).

- [2] B. L. Lev, E. R. Meyer, E. R. Hudson, B. C. Sawyer, J. L. Bohn, and J. Ye, Phys. Rev. A **74**, 061402 (2006).
- [3] H. L. Bethlem and W. Ubachs, Faraday Discuss. **142**, 25 (2009).
- [4] M. R. Tarbutt, J. J. Hudson, B. E. Sauer, and E. A. Hinds, Faraday Discuss. **142**, 37 (2009).
- [5] S. Y. T. van de Meerakker, N. Vanhaecke, M. P. J. van der Loo, G. C. Groenenboom, and G. Meijer, Phys. Rev. Lett. **95**, 013003 (2005).
- [6] J. J. Gilijamse, S. Hoekstra, S. Y. T. van de Meerakker, G. C. Groenenboom, and G. Meijer, Science **313**, 1617 (2006).
- [7] J. J. Gilijamse, S. Hoekstra, S. A. Meek, M. Metsälä, S. Y. T. van de Meerakker, G. Meijer, and G. C. Groenenboom, J. Chem. Phys. **127**, 221102 (2007).
- [8] W. C. Campbell, G. C. Groenenboom, H.-I. Lu, E. Tsikata, and J. M. Doyle, Phys. Rev. Lett. **100**, 083003 (2008).
- [9] R. V. Krems, Phys. Chem. Chem. Phys. **10**, 4079 (2008).
- [10] D. DeMille, Phys. Rev. Lett. **88**, 067901 (2002).
- [11] A. André, D. DeMille, J. M. Doyle, M. D. Lukin, S. E. Maxwell, P. Rabl, R. J. Schoelkopf, and P. Zoller, Nat. Phys. **2**, 636 (2006).
- [12] K. M. Jones, E. Tiesinga, P. D. Lett, and P. S. Julienne, Rev. Mod. Phys. **78**, 483 (2006).
- [13] T. Köhler, K. Góral, and P. S. Julienne, Rev. Mod. Phys. **78**, 1311 (2006).
- [14] J. D. Weinstein, R. deCarvalho, T. Guillet, B. Friedrich, and J. M. Doyle, Nature **395**, 148 (1998).
- [15] H. L. Bethlem and G. Meijer, Int. Rev. Phys. Chem. **22**, 73 (2003).
- [16] R. V. Krems, H. R. Sadeghpour, A. Dalgarno, D. Zgid, J. Kłos, and G. Chałasiński, Phys. Rev. A **68**, 051401 (2003).
- [17] W. C. Campbell, E. Tsikata, H.-I. Lu, L. D. van Buuren, and J. M. Doyle, Phys. Rev. Lett. **98**, 213001 (2007).
- [18] M. T. Hummon, W. C. Campbell, H.-I. Lu, E. Tsikata, Y. Wang, and J. M. Doyle, Phys. Rev. A **78**, 050702 (2008).
- [19] S. Y. T. van de Meerakker, R. T. Jongma, H. L. Bethlem, and G. Meijer, Phys. Rev. A **64**, 041401 (2001).
- [20] S. Hoekstra, M. Metsälä, P. C. Zieger, L. Scharfenberg, J. J. Gilijamse, G. Meijer, and S. Y. T. van de Meerakker, Phys. Rev. A **76**, 063408 (2007).

- [21] P. Soldán, P. S. Żuchowski, and J. M. Hutson, *Faraday Discuss.* **142**, 191 (2009).
- [22] A. O. G. Wallis and J. M. Hutson, *Phys. Rev. Lett.* **103**, 183201 (2009).
- [23] A. O. G. Wallis, E. J. J. Longdon, P. S. Żuchowski, and J. M. Hutson (2010), arXiv:1009.5505.
- [24] P. S. Żuchowski and J. M. Hutson, *Phys. Chem. Chem. Phys.* **13**, 3669 (2011).
- [25] M. T. Hummon, T. V. Tscherbul, J. Kłos, H.-I. Lu, E. Tsikata, W. C. Campbell, A. Dalgarno, and J. M. Doyle, *Phys. Rev. Lett.* **106**, 053201 (2011).
- [26] C. R. Monroe, E. A. Cornell, C. A. Sackett, C. J. Myatt, and C. E. Wieman, *Phys. Rev. Lett.* **70**, 414 (1993).
- [27] G. S. F. Dhont, J. H. van Lenthe, G. C. Groenenboom, and A. van der Avoird, *J. Chem. Phys.* **123**, 184302 (2005).
- [28] L. M. C. Janssen, G. C. Groenenboom, A. van der Avoird, P. S. Żuchowski, and R. Podeszwa, *J. Chem. Phys.* **131**, 224314 (2009).
- [29] C.-H. Lai, M.-D. Su, and S.-Y. Chu, *J. Phys. Chem. A* **107**, 2700 (2003).
- [30] T. V. Tscherbul, Y. V. Suleimanov, V. Aquilanti, and R. V. Krems, *New J. Phys.* **11**, 055021 (2009).
- [31] A. V. Avdeenkov and J. L. Bohn, *Phys. Rev. A* **64**, 052703 (2001).
- [32] J. Pérez-Ríos, M. Bartolomei, J. Campos-Martínez, M. I. Hernández, and R. Hernández-Lamonedá, *J. Phys. Chem. A* **113**, 14952 (2009).
- [33] M. Kajita, *Phys. Rev. A* **74**, 032710 (2006).
- [34] L. M. C. Janssen, P. S. Żuchowski, A. van der Avoird, G. C. Groenenboom, and J. M. Hutson, *Phys. Rev. A* **83**, 022713 (2011).
- [35] R. S. Ram and P. F. Bernath, *J. Mol. Spectrosc.* **260**, 115 (2010).
- [36] M. Mizushima, *The Theory of Rotating Diatomic Molecules* (Wiley, New York, 1975).
- [37] S. Green, *J. Chem. Phys.* **62**, 2271 (1975).
- [38] M. H. Alexander and D. E. Manolopoulos, *J. Chem. Phys.* **86**, 2044 (1987).
- [39] J. M. Hutson and S. Green, MOLSCAT computer code, version 14 (1994), distributed by Collaborative Computational Project No. 6 of the Engineering and Physical Sciences Research Council (UK).
- [40] M. L. González-Martínez and J. M. Hutson, *Phys. Rev. A* **75**, 022702 (2007).
- [41] *MATLAB Version 7.9*, The MathWorks, Inc. (2009), <http://www.mathworks.com>.
- [42] E. P. Wigner, *Phys. Rev.* **73**, 1002 (1948).

[43] R. V. Krems and A. Dalgarno, Phys. Rev. A **67**, 050704 (2003).

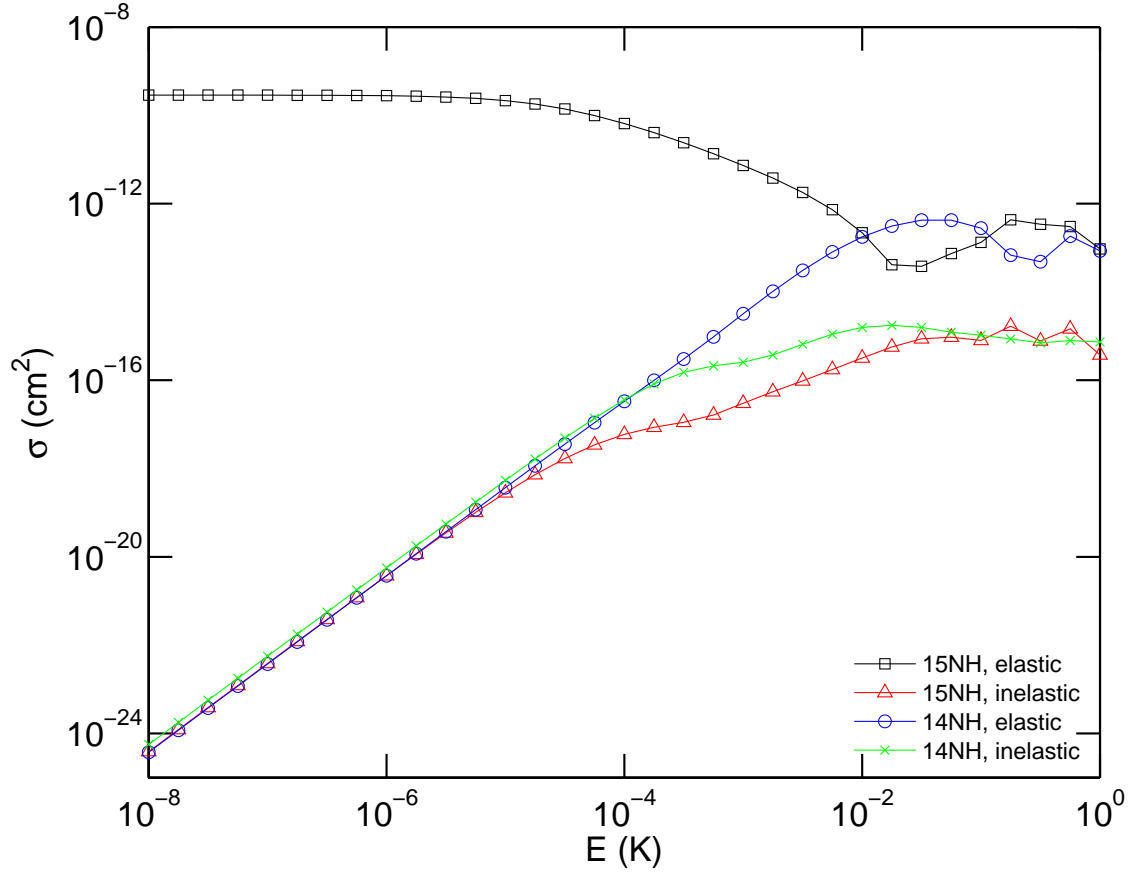


FIG. 1: Elastic and inelastic M_J -changing cross sections for $^{14}\text{NH} + ^{14}\text{NH}$ and $^{15}\text{NH} + ^{15}\text{NH}$ collisions, assuming that all molecules are in their magnetically trappable and nuclear-spin stretched state.

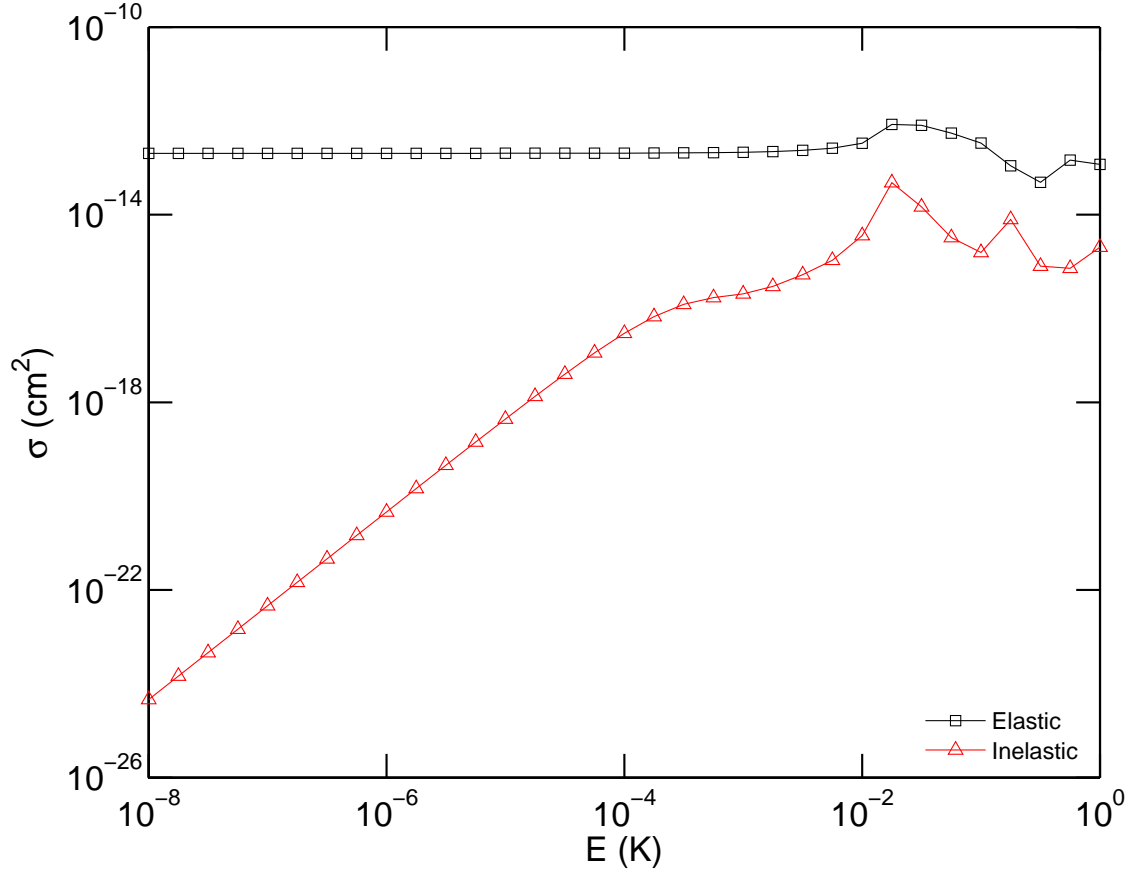


FIG. 2: Elastic and inelastic M_J -changing cross sections for magnetically trapped ^{14}NH , assuming a statistical mixture of nuclear-spin states.

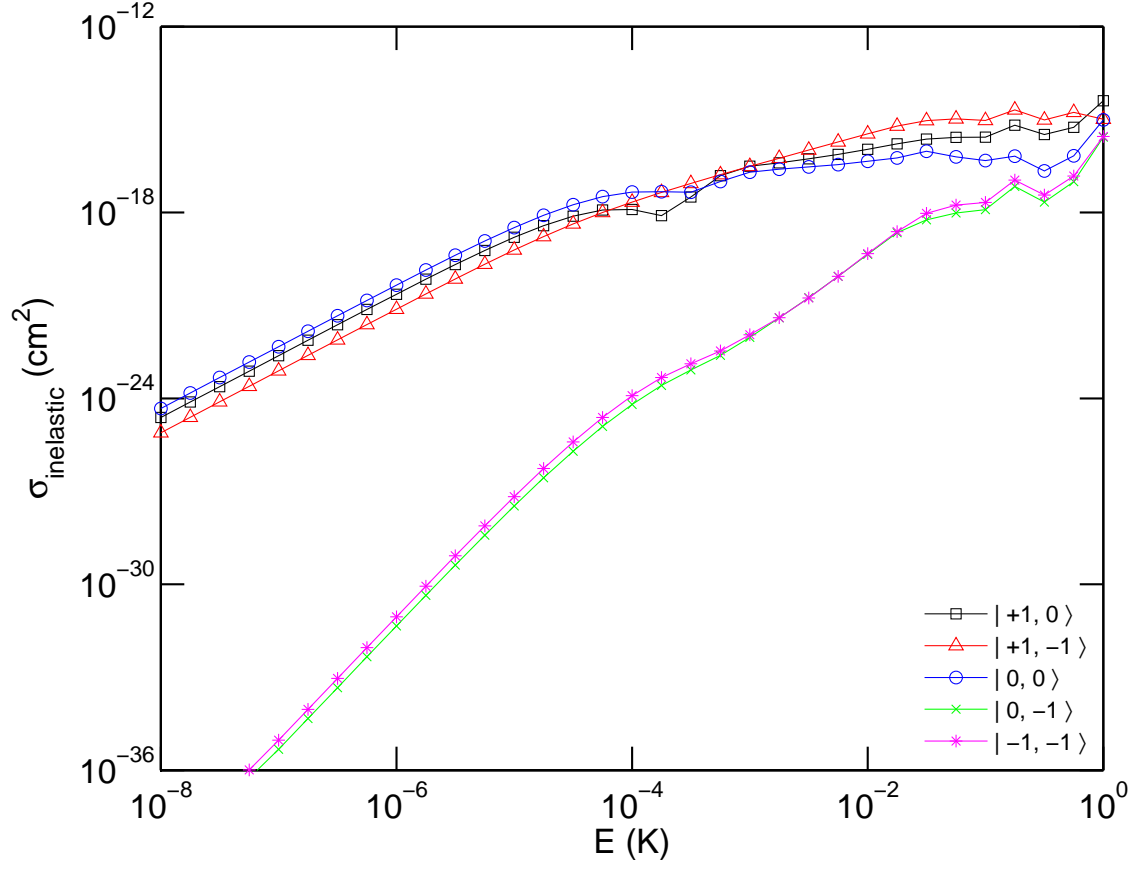


FIG. 3: State-to-state inelastic cross sections for magnetically trapped ^{15}NH as a function of collision energy. The final states are labeled by $|M_{J_A}, M_{J_B}\rangle$.

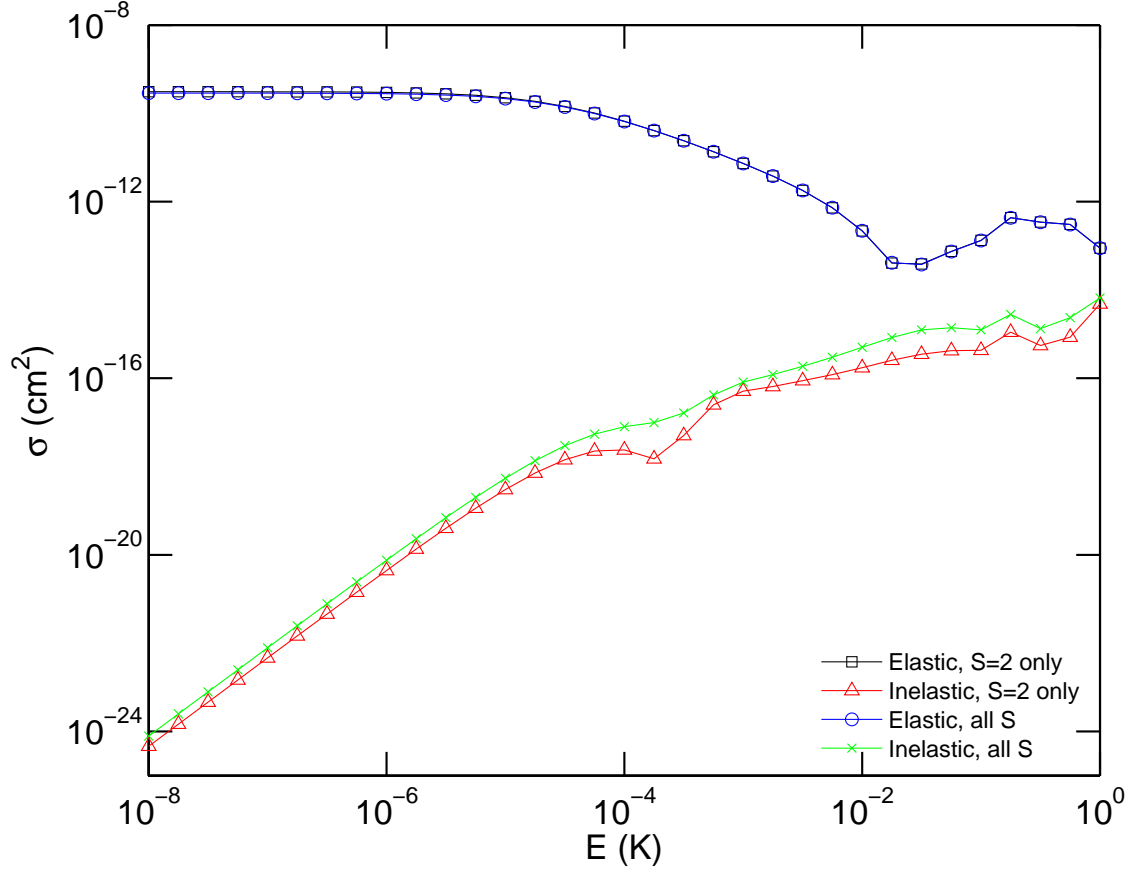


FIG. 4: Elastic and inelastic M_J -changing cross sections for magnetically trapped ^{15}NH obtained from scattering calculations with only the quintet state included in the basis. The cross sections calculated with all three spin states included (“all S ”) are shown for comparison.

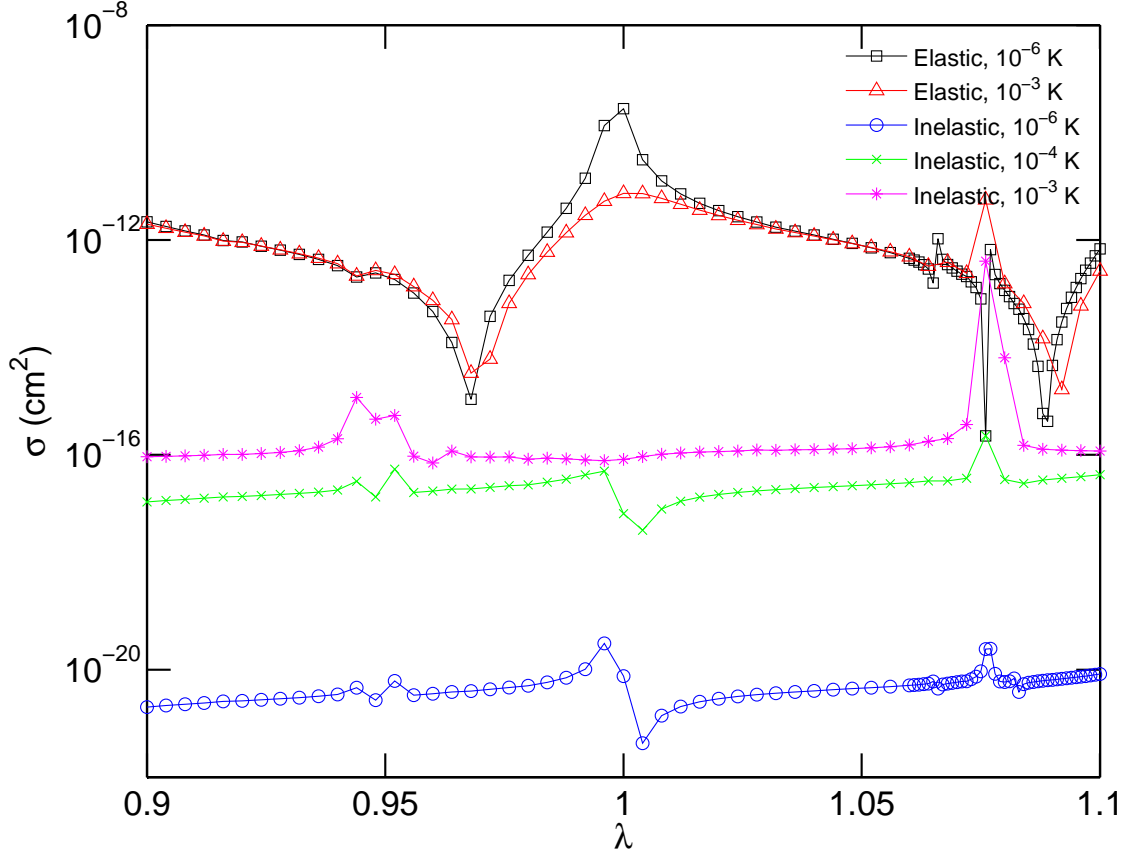


FIG. 5: Elastic and inelastic M_J -changing cross sections for magnetically trapped ^{15}NH as a function of the scaling parameter λ , calculated at collision energies of 10^{-6} K, 10^{-4} K, and 10^{-3} K. The elastic cross sections for 10^{-4} K are the same as for 10^{-6} K.

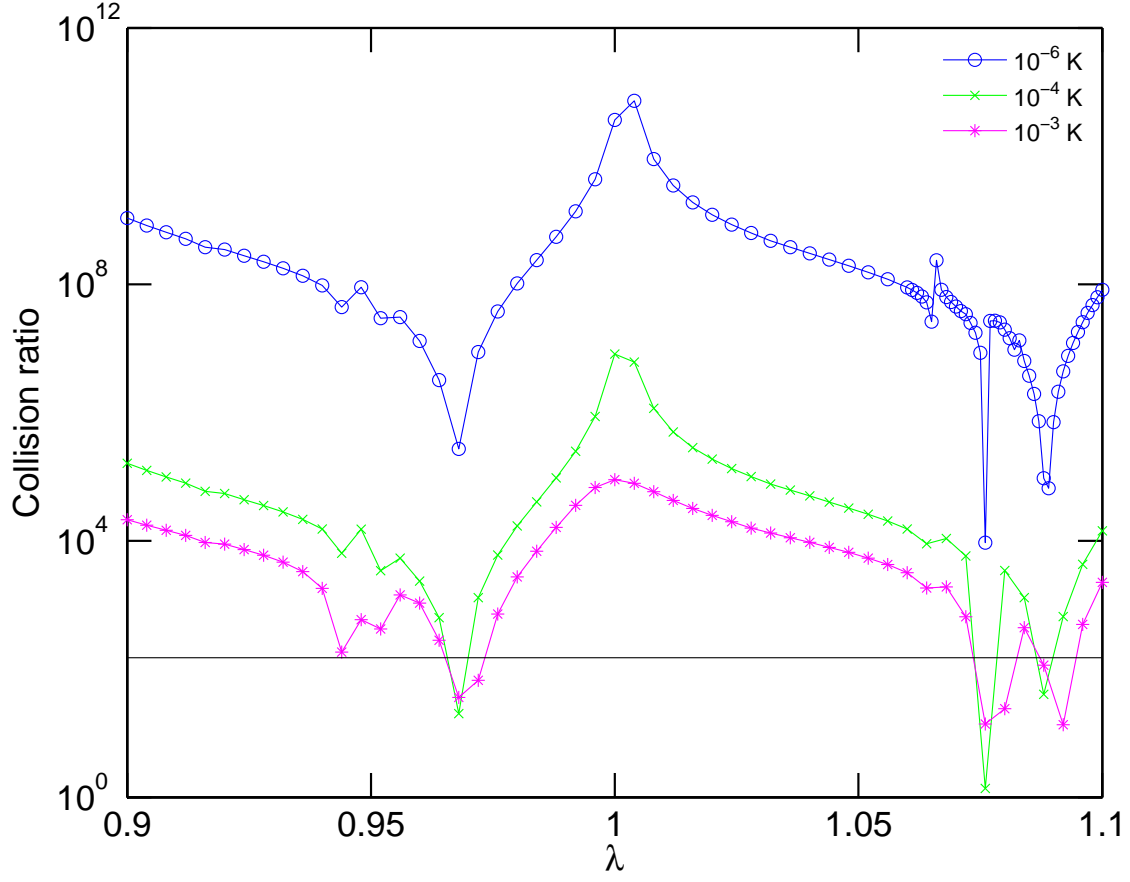


FIG. 6: Elastic-to-inelastic cross-section ratios for magnetically trapped ^{15}NH as a function of the scaling parameter λ , calculated at collision energies of 10^{-6} K, 10^{-4} K, and 10^{-3} K. The horizontal black line indicates the critical value of 150 that is required for efficient evaporative cooling.

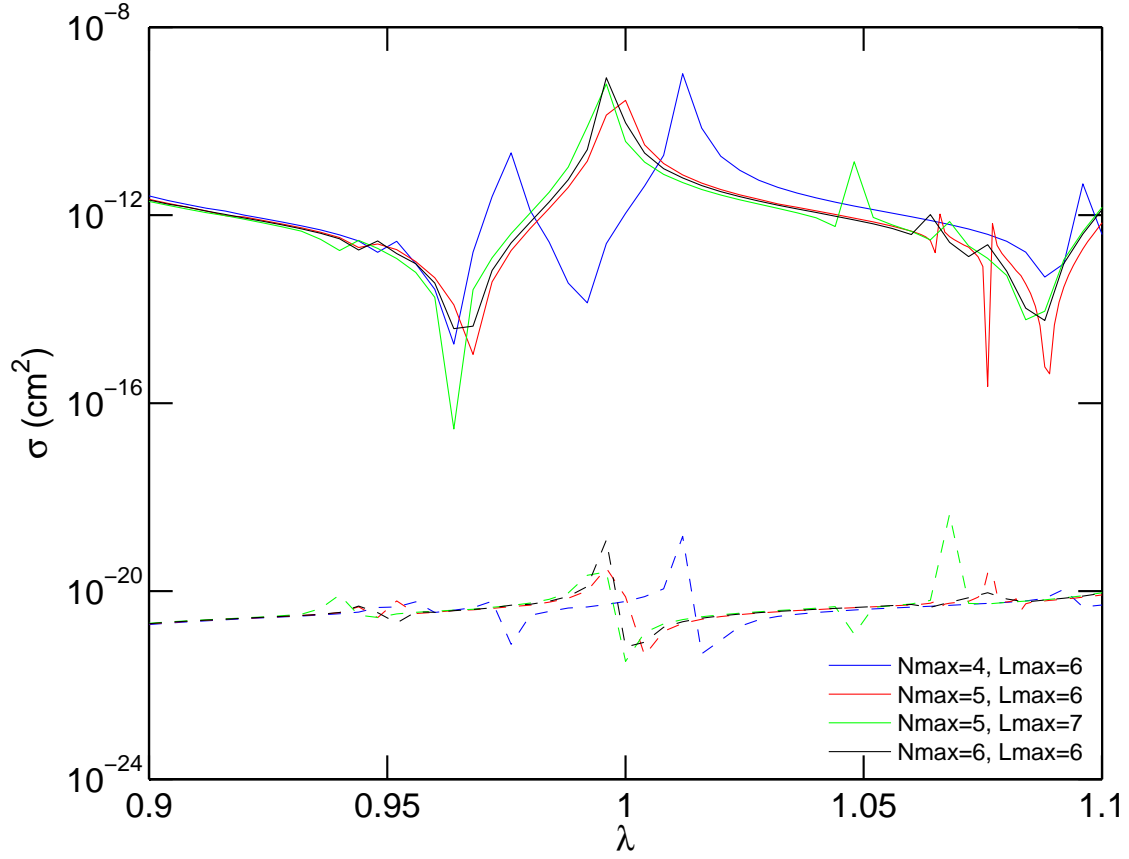


FIG. 7: Elastic and inelastic M_J -changing cross sections for magnetically trapped ^{15}NH as a function of λ , calculated for different basis sets at a collision energy of 10^{-6} K. Solid lines correspond to elastic cross sections and dashed lines to inelastic cross sections. Different colors represent different basis sets.